1 **Modulation of protein-DNA binding reveals mechanisms of spatiotemporal gene control in**

2 **early *Drosophila* embryos**

3 Sahla Syed[1], Yifei Duan[1,2], and Bomyi Lim[1]*

4 [1] Department of Chemical and Biomolecular Engineering, University of Pennsylvania,

5 Philadelphia, PA 19104

6 [2] Master of Biotechnology Program, University of Pennsylvania, Philadelphia, PA 19104

7 * To whom correspondence may be addressed: bomyilim@seas.upenn.edu

8 **Abstract**

9 It is well known that enhancers regulate the spatiotemporal expression of their target genes by

10 recruiting transcription factors (TFs) to the cognate binding sites in the region. However, the role

11 of multiple binding sites for the same TFs and their specific spatial arrangement in determining

12 the overall competency of the enhancer has yet to be fully understood. In this study, we utilized

13 the MS2-MCP live imaging technique to quantitatively analyze the regulatory logic of the *snail*

14 distal enhancer in early *Drosophila* embryos. Through systematic modulation of Dorsal and Twist

15 binding motifs in this enhancer, we found that a mutation in any one of these binding sites causes

16 a drastic reduction in transcriptional amplitude, resulting in a reduction in total mRNA production

17 of the target gene. We provide evidence of synergy, such that multiple binding sites with moderate

18 affinities cooperatively recruit more TFs to drive stronger transcriptional activity than a single site.

19 Moreover, a Hidden Markov-based stochastic model of transcription reveals that embryos with

20 mutated binding sites have a higher probability of returning to the inactive promoter state. We

21 propose that TF-DNA binding regulates spatial and temporal gene expression and drives robust

22 pattern formation by modulating transcriptional kinetics and tuning bursting rates.

23 **Key words**

24 Transcription kinetics; live imaging; MS2-MCP; transcription factors; bursting; Hidden Markov

25 model

26

27 **Introduction**

28 Development of a *Drosophila* embryo is a highly precise and coordinated process, occurring with

29 little variability despite intrinsic and extrinsic noise and perturbations (Arias and Hayward 2006;

30 Houchmandzadeh, Wieschaus, and Leibler 2002). Proper levels of essential genes and correct

31 positioning of expression patterns are regulated by short non-coding DNA sequences known as

32 enhancers (Banerji, Rusconi, and Schaffner 1981). Enhancers tightly control their target gene

33 expression both in space and time via transcription factor (TF) recruitment. Complex patterning

34 and cell fates are established through TFs recognizing and binding to specific short DNA

35 sequences within enhancers with varying degrees of affinity at different developmental stages

36 (Long, Prescott, and Wysocka 2016; Reiter, Wienerroither, and Stark 2017; Ramos and Barolo

37 2013b). Concerted action of TFs with other transcriptional machinery has been found to reposition

38 nucleosomes, initiate chromatin remodeling, recruit additional activating co-factors, and generate

39 distinct transcriptional outputs (Spitz and Furlong 2012). However, it remains to be understood

40 how these brief, yet frequent, interactions between TFs and regulatory DNAs facilitate efficient

41 and specific transcription on the timescale of minutes. Although we know that TFs influence

42 various facets of transcription such as timing or probability of activation, we have yet to determine

43 their role in orchestrating an enhancer's transcriptional competency at a mechanistic level. For

44 example, does the spatial arrangement of the binding sites influence transcriptional capability?

45 How does each TF binding site shape transcriptional dynamics of individual nuclei and contribute

46 to overall pattern formation?

47   Recently, it was shown that the genomic context of an enhancer provides an optimal environment

48   for driving normal expression patterns and preventing misregulation upon induced perturbations.

49   Mutating a single Giant repressor binding site in a minimal *even-skipped* stripe 2 enhancer region

50   caused misexpression of the target gene, whereas those effects were buffered in an extended

51   enhancer containing more TF binding sites and expression levels were comparable to the wildtype

52   (López-Rivera et al. 2020). However, the role of multiple TF binding sites with varying affinities

53   within the enhancer in regulating transcription has yet to be established. Recent studies have

54   explored the role of low-affinity binding sites in producing specific expression patterns and found

55   that enhancers containing optimal TF motifs may lead to overexpression and result in

56   developmental defects (Farley et al. 2015; Ramos and Barolo 2013a; Tsai et al. 2017). Previous

57   work has shown that modulating the strength of a single TF binding site was sufficient to disrupt

58   transcriptional activity, such that a mutation of an activator Dorsal (Dl) site in the *t48* enhancer

59   delayed activation and almost completely abolished transcriptional activity, while optimization of

60   the site to a consensus motif induced ectopic transcriptional activity with a broader gene

61   expression domain (Keller et al. 2020). However, systematic removal of binding sites of varying

62   affinities for another activator Bicoid seems to affect its target gene, *hunchback*, expression to a

63   similar degree, indicating that each site has a nearly equal contribution to the overall expression

64   pattern (Eck et al. 2020). Yet, since many studies have relied on fixed tissue experiments to derive

65   the role of TFs in transcriptional regulation, the changes in real-time transcription kinetics that

66   drive the observed misexpression are often overlooked. Dynamic interplay among TFs, cofactors,

67   and DNA occurs on the order of seconds, a time resolution that cannot be resolved solely through

68   RNAi and single molecule *in situ* hybridization experiments (Mir et al. 2017). Since TF binding

69   events affect the expression of regulatory genes both spatially and temporally, incorporation of

70   both live imaging techniques and predictive modeling is crucial to correlate transient TF-DNA

71   binding to downstream transcriptional activity in single-cell resolution.

72   In this study, we investigated the effects of perturbing TF-DNA binding strength on the

73   transcriptional dynamics of *snail* (*sna*) in early *Drosophila* embryos. *sna* is a well-characterized,

74   key patterning gene that encodes a zinc finger protein and is responsible for the differentiation of

75   the mesoderm (Rembold et al. 2014; Ip et al. 1992; Leptin 1991). Sna represses the expression

76   of genes responsible for neuroectoderm formation and establishes the mesoderm-neuroectoderm

77   boundary (Kosman et al. 1991). Embryos lacking *sna* fail to undergo gastrulation, resulting in

78   embryonic lethality (Hemavathy et al. 2004). Previous studies have demonstrated that *sna*

79   expression is controlled by a proximal enhancer and a distal (shadow) enhancer located directly

80   upstream and ~7 kb upstream of the promoter, respectively (Perry et al. 2010). The distal

81   enhancer is necessary for proper *sna* expression and the viability of the developing embryo,

82   especially under genetic and environmental stresses (Perry et al. 2010; Dunipace, Ozdemir, and

83   Stathopoulos 2011). *sna* is a target gene of the Dl morphogen, and the nuclear gradient of

84   maternally deposited Dl protein controls the sharp boundaries of *sna* expression, such that only

85   nuclei with high concentrations of nuclear Dl express *sna* (Figure 1B) (Hong et al. 2008). Through

86   binding assays like EMSA and ChIP-seq, it was determined that the distal *sna* enhancer contains

87   multiple, low affinity binding sites for Dl, Twist (Twi), and the pioneer factor Zelda (Zld) (Figure

88   1A) (Zeitlinger et al. 2007; Ferraro et al. 2016). Indeed, *sna* expression is completely abolished in

89   embryos lacking Dl or Twi, and Zld null embryos show a delay in *sna* activation (Dufourt et al.

90   2018; Liang et al. 2008).

91   Here, we utilize a combination of quantitative live imaging and mathematical modeling to probe

92   the underlying regulatory mechanisms that TFs employ to initiate transcription, regulate gene

93   expression levels, and establish spatial boundaries. Using MS2-MS2 coat protein (MCP) based

94   live imaging, we visualized transcription dynamics driven by the wildtype minimal *sna* distal

95   enhancer in the cases of with and without various TF binding site mutations. We find that mutating

96   a single TF (Dl or Twi) binding site in the enhancer significantly reduces mRNA production of the

97   target gene, mainly by lowering transcriptional amplitude, without significantly delaying the timing

98   of initiation or affecting the probability of activation. Surprisingly, we found that modulating the

99   same TF binding site in the context of the full *sna* distal enhancer results in a similar reduction in

100   expression levels, underscoring that additional TF binding sites in the full enhancer are not

101   sufficient to rescue reduced transcriptional activity. Using a thermodynamic equilibrium binding

102   model, we show that the TF binding sites must cooperate with each other to establish the correct

103   spatial pattern of *sna*. Moreover, a two-state stochastic model of transcription indicates that TF

104   binding site mutations affect transcriptional bursting, specifically by increasing the probability of

105   the promoter switching out of the ON state, k_{off}, and reducing burst durations. Together, our data

106   highlight the distinct mechanisms by which TF binding sites regulate transcriptional kinetics and

107   spatial patterning during embryonic development.

108   **Results**

109   **Single TF binding site mutation greatly diminishes the transcriptional capability of the**

110   **distal *sna* enhancer**

111   The 519 bp *sna* minimal enhancer is located within the full *sna* distal enhancer (1.8 kb) and has

112   been shown to recapitulate proper *sna* expression (Figure 1A) (Ferraro et al. 2016). We focus on

113   the analysis of the minimal enhancer since it contains fewer TF binding sites than the full distal

114   enhancer, which allows systematic perturbation in a sensitized background to gain a functional

115   understanding of the role of TF binding site arrangements in gene regulation. The minimal

116   enhancer contains binding sites for many TFs, including Dl, Twi, and Zld, and our study focuses

117   on the sites with the strongest binding affinities, three Dl sites and one Twi site (Figure 1A). We

118   note that all Dl and Twi sites still have relatively low binding affinities compared to the consensus

119   motif, because *sna* is activated only in the domain with high nuclear Dl concentration (Hong et al.

120   2008). We systematically deleted one site at a time by introducing point mutations in each binding

121   motif. The mutations were created by inducing double-nucleotide substitutions that cause the

122   sequence to no longer be recognized as a TF motif match (Table 1).

123

124   We utilized the MS2-MCP live imaging technique to quantitatively analyze the effects of

125   modulating TF binding sites within the minimal *sna* distal (sna*min*) enhancer. Specifically, the 10x

126   repeat sequences of MS2 are integrated into the 5' UTR of the *yellow* reporter gene (Figure 1A).

127   Upon transcription, each MS2 sequence forms a stem loop which is detected by maternally

128   deposited MCP tagged with fluorescent proteins. To visualize nascent transcription dynamics,

129   females carrying His2Av-mRFP and MCP-GFP were crossed with males carrying the desired

130   MS2 construct, resulting in progeny expressing distinct fluorescent puncta in active transcription

131   loci (Figure 1C, Video 1). *sna* distal enhancer drives gene expression in the endogenous *sna*

132   domain, where the nuclear Dl level is the highest (Figure 1B). The fluorescence intensity trajectory

133   for each nucleus is extracted for subsequent analysis and correlated to its instantaneous

134   transcriptional activity (Figure 1D,E).

135

136   We found that a mutation of any single Dl or Twi binding site within the minimal enhancer resulted

137   in a dramatic reduction in mRNA production (Figure 1F, Video 1,2, Figure 1 supplement 1A).

138   Nuclei in the center of the *sna* expression domain of a mutant embryo produce 65% less mRNA

139   than those in the wildtype counterpart. The reduction occurs uniformly across the *sna* expression

140   domain without significantly affecting the width (Figure 1G, Figure 1 supplement 1C). It is

141   important to note that mutations of different TFs (Dl and Twi) and of binding sites with different

142   affinities (Dl1 and Dl2) all result in a similar degree of decreased mRNA production. Surprisingly,

143   even the embryos with two mutated binding sites exhibit a similar mRNA reduction (Figure 1G –

144   pink, Figure 1 supplement 1A - orange). These results suggest that each site in the minimal

145   enhancer is necessary to drive normal *sna* expression, perhaps due to the sensitized background

146   in which the mutations were induced.
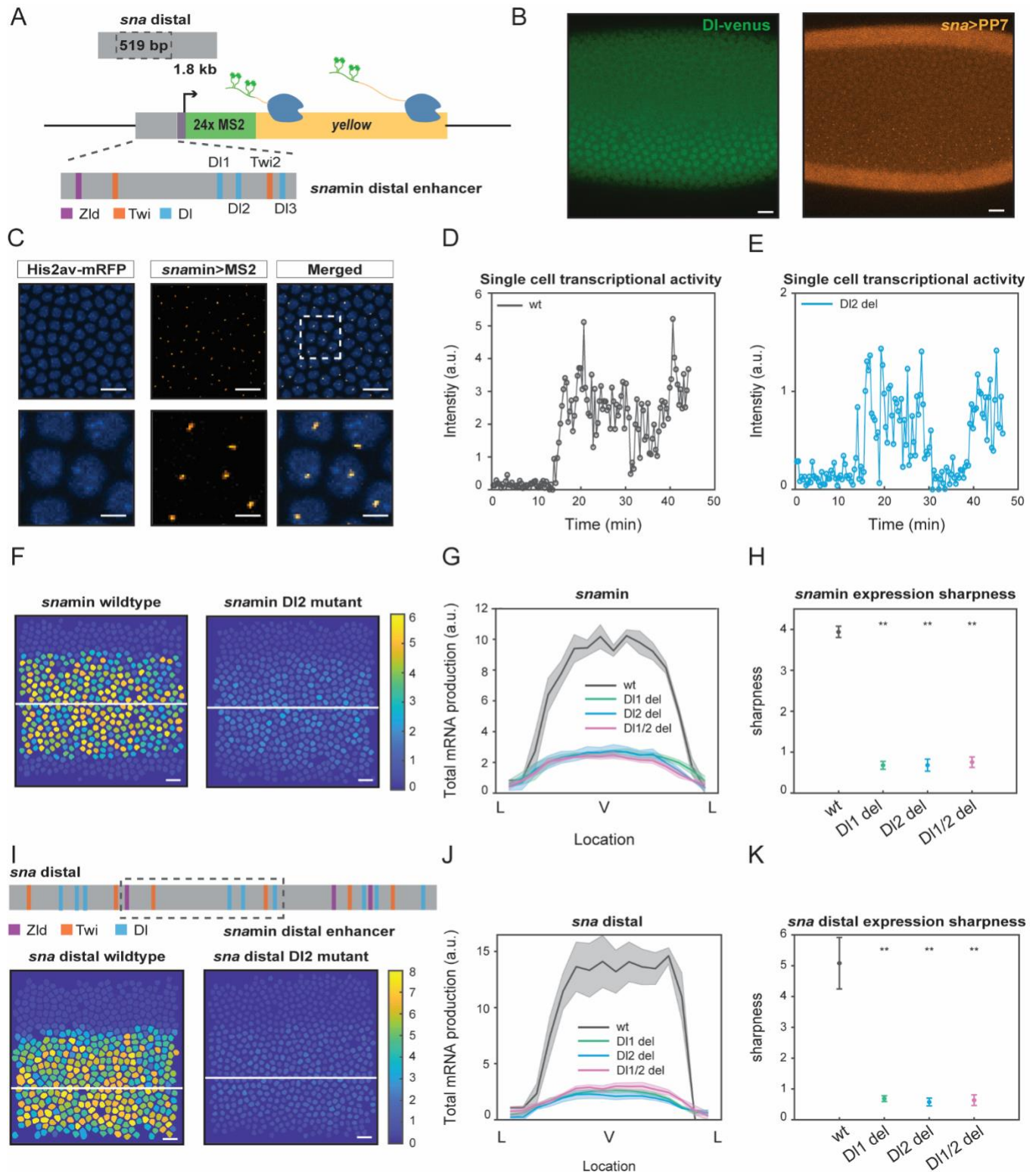
Figure 1. Single TF binding site mutation greatly diminishes mRNA production from the distal *sna* enhancer

(A) Schematic of the reporter construct containing the minimal *sna* distal enhancer, *sna* core promoter, MS2 stem loops, and the *yellow* reporter gene. The minimal enhancer contains binding sites for TFs Zld, Twi, and Dl.

(B) Embryo expressing maternally deposited Dl-Venus protein (green) and *sna* distal>*PP7-yellow* reporter gene (orange). *sna* is expressed in the region with high nuclear Dl.

(C) Snapshots of an embryo expressing minimal *sna* distal>*MS2-yellow*. The nuclei are marked with Histone-RFP (blue) and the MS2-*yellow* reporter gene is observed with MCP-GFP (orange). Each nucleus has one distinct fluorescent punctum, indicating nascent transcription. Bottom row are magnifications of the embryo within the rectangle.

(D,E) Single nucleus transcriptional trajectories for a wildtype and Dl2 mutant embryo, respectively.

(F) Heatmap showing that mRNA production is higher in a wildtype embryo compared to a Dl2 mutant embryo. The white line indicates the ventral midline.

(G) Average mRNA production of all nuclei in wildtype embryos and Dl1, Dl2, and Dl1/2 mutant embryos across the *sna* expression domain (Lateral-Ventral-Lateral).

(H) Plot indicating the wildtype steepness of *sna*min expression is significantly higher than the mutants.

(I) Top: Schematic showing the additional TF binding sites present in the full *sna* distal enhancer. Bottom: Heatmap showing higher mRNA production of *MS2-yellow* in a wildtype embryo containing the full *sna* distal enhancer compared to the embryo containing the full enhancer with Dl2 site mutations.

(J) Average mRNA production of all nuclei in wildtype embryos and Dl1, Dl2, and Dl1/2 mutant embryos containing the full *sna* distal enhancer across the expression domain.

(K) Plot indicating the wildtype steepness of *sna* distal expression is significantly higher than the mutants.

Shaded error bars in (E), (G), and (J) indicate standard error of the mean (SEM).

Error bars in (H) and (K) indicate SEM.

1524 nuclei from 3 replicate wildtype embryos, 1672 nuclei from 4 replicate Dl1 mutant embryos, 2091 nuclei from four replicate Dl2 mutant embryos, and 1788 nuclei from three replicate Dl1/2 mutant embryos were analyzed.

** denote p<0.001 from the student's t-test.

147

148   To further examine the significance of these core TF binding sites in the minimal enhancer, we

149   investigated if the additional TF binding sites in the full distal enhancer would buffer against the

150   drastic changes in mRNA production caused by the mutations. Despite several additional Dl and

151   Twi sites flanking the minimal enhancer, we found that the same mutations on the same TF motifs

152   caused a similar decrease in mRNA production (Figure 1I,J). Furthermore, we found that in both

153   the minimal and full distal enhancers, the mutant embryos have shallower gradients and less

154   sharp boundaries, highlighting the importance of proper TF-DNA interactions in regulating the

155   sharpness of the expression domain (Figure 1H,K, Figure 1 supplement 1B). Shallower

156   expression of *sna* may lead to higher uncertainty in germ layer formation between mesoderm and

157   neuroectoderm. It is interesting to note that the introduction of the mutations in the larger genomic

158   context (i.e., full distal enhancer) did not lessen their effect on transcriptional activity and pattern

159   formation. Here, it is evident that additional TF sites are not able to rescue normal *sna*

160   transcriptional activity and that each site within the minimal enhancer region plays a critical role

161   in ensuring robust expression.

162

163   **Mutations cause lower mRNA production, mainly due to reduced transcriptional amplitude**

164   After establishing the dramatic reduction in transcriptional activity, we delved into the underlying

165   causes of the low mRNA production in both a single nucleus and across the entire *sna* expression

166   domain. We hypothesized that the reduced mRNA production may occur through multiple different

167   modes. The mutations may affect the transcriptional capability of the enhancer by altering the

168   time of transcriptional activation or by reducing the transcriptional window, thereby effectively

169   lowering the mRNA production compared to a wildtype embryo. Or the mutations may reduce the

170   enhancer's ability to transcribe and effectively load Pol II, resulting in decreased instantaneous

171   transcriptional amplitude (Figure 2A). We found that the differences in the time for half the nuclei
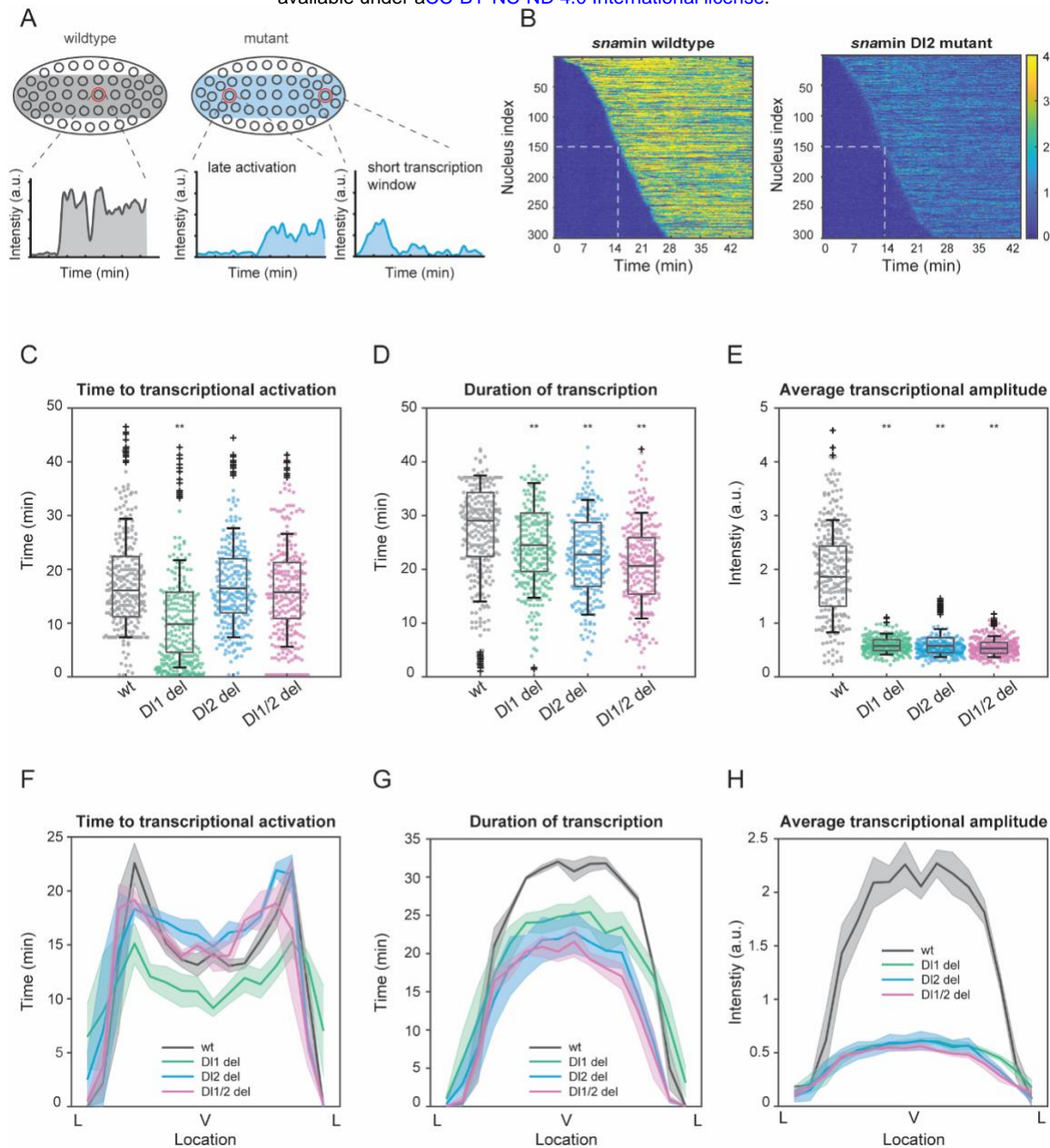
Figure 2. Mutations cause lower mRNA production, mainly due to lower transcriptional amplitude

(A) Schematic comparing wildtype and mutants. The mutant embryo may have fewer nuclei transcribing and at a lower intensity. Each nucleus in mutant embryos may have late activation or a shorter transcription window, all of which may contribute to the observed low mRNA production.

(B) Heatmap of transcription activation times for representative wildtype and Dl2 mutant embryos. The time at which half of the nuclei are activated is indicated by the dotted white line and there is no significant difference.

(C-E) Boxplots showing (C) the time to transcriptional activation (D) the duration of active transcription, and (E) the transcriptional amplitude for all actively transcribing nuclei. Decreased transcriptional amplitude contributes the most to the low mRNA production in mutants.

(F-G) (F) Average time to transcriptional activation, (G) average duration of transcription for all actively transcribing nuclei, and (H) average transcriptional amplitude for all nuclei across the *sna* expression domain (Lateral – Ventral – Lateral). Nuclei in the middle of the expression domain are affected more, but there is no significant change in the expression width.

Shaded error bars in (F-H) indicate SEM.

250 individual data points are overlaid on the respective boxplots.

1124 nuclei from 3 replicate wildtype embryos, 1011 nuclei from 4 replicate Dl1 mutant embryos, 1123 nuclei from four replicate Dl2 mutant embryos, and 943 nuclei from three replicate Dl1/2 mutant embryos were analyzed.

Transcription of the *MS2-yellow* reporter gene is driven by the minimal *sna* distal enhancer.

** denote p<0.001 from the student's t-test.

172   to begin transcription as well as the transcription initiation time per nucleus were not sufficient to

173   explain the low mRNA output (Figure 2B,C, Figure 2 supplement 1A). Although the duration of

174   active transcription is slightly lowered in embryos containing the induced mutations (Figure 2D,

175   Figure 2 supplement 1B), the main cause of the low mRNA output was the average transcriptional

176   amplitude (Figure 2E, Figure 2 supplement 1C). Here, we observed a significant decrease in

177   transcriptional intensity, leading us to conclude that the mutations mainly modulate transcription

178   by lowering Pol II loading rate. At single-cell resolution, we find that the mutants with two deleted

179   binding sites have a slightly bigger impact on transcriptional activity than those with one site

180   removed, but the differences are minimal (Figure 2C-E, Figure 2 supplement 1A-C).

181

182   Since *sna* is a patterning gene and is responsible for the formation of the ventral furrow and

183   presumptive mesoderm, we wanted to determine how the mutations spatially affect the

184   aforementioned transcription parameters and the spatial boundaries of the expression pattern.

185   The nuclei in the center of the *sna* expression domain are more substantially affected, exhibiting

186   lower duration of transcription and average transcriptional amplitude, confirming the trend we

187   observed for mRNA production (Figure 2F,G, Figure 2 supplement 1D-F). Our results agree with

188   previous studies, in which the center nuclei within the *eve* stripe 2 domain had significantly longer

189   transcription windows and overall, higher rates of mRNA production (Lammers et al. 2020).

190   Interestingly, we observed that the Dl1 mutation induced earlier transcriptional activation than

191   wildtype (Figure 2C,F). Since the Dl1 and Dl2 binding sites are less than 10 bp apart, mutating

192   the Dl1 site may create a more favorable steric conformation, allowing Dl to bind to the single site

193   more efficiently. However, the earlier activation time is not sufficient to buffer against the severe

194   reduction in transcriptional amplitude and causes the Dl1 mutant to exhibit similarly reduced

195   mRNA production (Figure 1G).

196

197 Interestingly, in addition to modulating the average transcriptional intensity, the mutations in the

198 full distal enhancer affect the time to activation and the transcription window as well.

199 Transcriptional activation is more significantly delayed and the duration of transcription is

200 substantially lower in the mutants than in the wildtype (Figure 2 supplement 2A-C). As with the

201 case with the minimal enhancer, here we do not observe any significant spatial modulation of

202 these parameters and the expression width remains unaffected (although the boundary is less

203 sharp) (Figure 2 supplement 2D-F).

204

205 **Thermodynamic equilibrium binding model reveals synergistic interactions among TF**

206 **binding sites**

207 The mechanistic role that multiple TF binding sites with different affinities play in regulating

208 enhancer activity and capability is still unclear. Is a single binding site sufficient to establish the

209 correct pattern and expression levels? In that case, why does an enhancer contain multiple TF

210 binding sites for the same TF? Our findings seem to indicate a nonadditive behavior between

211 binding sites, such that both a single and double mutation affect transcriptional dynamics to a

212 similar degree. We utilized a thermodynamic Monod-Wyman-Changeux (MWC) model to examine

213 the contributions of each Dl and Twi site to the overall competency of the enhancer (Monod,

214 Wyman, and Changeux 1965). Here, we assume that the microstates (unbound, bound with

215 activator(s)) are in equilibrium and that the probability of each state can be correlated with its

216 Boltzmann weight (Eck et al. 2020). As described in (Eck et al. 2020; Kanodia et al. 2012), the

217 Boltzmann weights can be calculated in terms of activator concentration C, dissociation constant,

218 K, and a cooperativity term ω (Figure 3A). The probability of transcription initiation is represented

219 by the probability of an activator (i.e., Dl) binding to its cognate site, which can be written as:

220
$$p_{bound} = \frac{\frac{C_{Dl1}}{K_{Dl1}} + \frac{C_{Dl2}}{K_{Dl2}} + \omega \frac{C_{Dl1} C_{Dl2}}{K_{Dl1} K_{Dl2}}}{1 + \frac{C_{Dl1}}{K_{Dl1}} + \frac{C_{Dl2}}{K_{Dl2}} + \omega \frac{C_{Dl1} C_{Dl2}}{K_{Dl1} K_{Dl2}}}$$
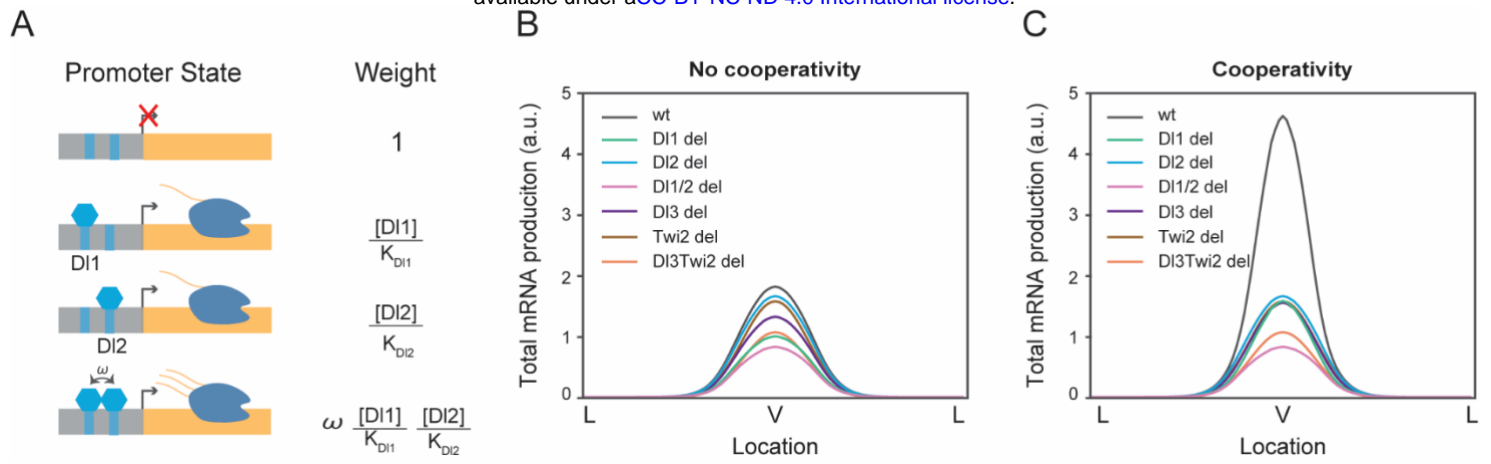
Figure 3. Thermodynamic equilibrium binding model reveals synergy among TF binding sites

(A) Promoter states and statistical weights for each microstate. A bound activator will yield transcription. Cooperativity term ω is included when more than one TF is bound which will result in higher mRNA production. Dissociation constants are given by K_i, which is correlated with the binding affinity of each site.

(B-C) mRNA production curves generated by assuming (B) no cooperativity and (C) cooperativity among TF binding sites. Modeling results support experimental data with the cooperativity term included.

221

222   This equation can be expanded to include all the combinations of Dl and Twi interactions (See

223   Methods, Equation 1). The equilibrium binding constants were correlated to the p-values

224   calculated from the PWM scanning software, FIMO (Bailey et al. 2015) (see Methods). We first

225   tested our model in the case of completely independent binding, or no cooperativity. In this

226   condition, the model failed to predict the experimental data and we found that the wildtype has

227   only slightly higher expression levels compared to the mutants (Figure 3B). When we modified

228   the model to include the cooperativity terms among all the TFs, we were able to qualitatively

229   recapitulate the experimental mRNA production curve as well as determine which TFs work

230   synergistically to help recruit more TFs to the enhancer region (Figure 3C). We found that

231   Dl1/Dl2/Twi, Dl2/Dl3/Twi, and Dl1/Dl2/Dl3/Twi cooperativities were the key parameters to reach

232   a stable solution, confirming the role of cooperativity among weak binding sites as a mechanism

233   for precise gene control. We note that the deletion of one or two sites would render no

234   cooperativity, and hence would result in a similar effect on transcription. Our data demonstrate

235   that TF binding sites must coordinate with one another to some degree to recreate the correct

236   pattern and levels of *sna*. Synergistic interactions among TFs have been observed in other genes

237   as well, such that the transcriptional output of multiple TFs is significantly higher than the sum of

238   their individual activities (Keller et al. 2020; Park et al. 2019). We propose that the cooperativity

239   allows TF binding sites with moderate or weak affinities to recruit more TFs to the enhancer,

240   generate sharp transcriptional responses, and drive strong and robust expression in the narrow

241   *sna* expression domain (see Discussion).

242

243   **A two-state model of transcription reveals differences in** k_{off} **rates and burst duration**

244   As shown previously, transcription occurs discontinuously in distinct, stochastic bursts of activity

245   punctuated by quiescence (Corrigan et al. 2016; Senecal et al. 2014; Donovan et al. 2019).

246   Bursting has been proposed as an evolutionary mechanism for driving heterogeneity in gene

247 expression, giving rise to cell-to-cell variability and overall diversity (Rodriguez and Larson 2020).

248 Bursting parameters, such as burst frequency, burst duration, and promoter switching rates

249 provide a glimpse into the underlying mechanisms of dynamic transcription regulation, such as

250 kinetic rates and promoter states. We find that the wildtype and mutant embryos show comparable

251 numbers of actively transcribing nuclei at the beginning of the nuclear cycle 14. However, at later

252 times, most wildtype nuclei in the *sna* expression domain are active in a given frame while nuclei

253 from mutant embryos exhibit stochastic activity (Figure 4A, Video 3,4). Indeed, by quantifying the

254 number of nuclei transcribing at every time point, we find that the embryos with mutations have

255 far fewer active nuclei in each frame compared to the wildtype, despite their cumulative number

256 of active nuclei being comparable (Figure 4 supplement 1A,B). We use stochastic modeling of

257 transcription to investigate if TF binding site mutations cause changes in transcriptional bursting

258 characteristics of each nucleus. The two-state model, in which a promoter can switch between an

259 active (ON) and inactive (OFF) state, has been widely implemented to gain a functional

260 understanding of bursting control on transcription (Figure 4B) (Bothma et al. 2014; Corrigan et al.

261 2016).

262

263 Hidden Markov models (HMMs) are utilized to reveal hidden states not directly observable based

264 on a sequence of observed events (Bronson et al. 2009). They are extensively used to recover

265 rates of promoter switching and other bursting parameters from transcriptional trajectories

266 (Bothma et al. 2014; Lammers et al. 2020; Hoppe et al. 2020). In this study, we utilize an HMM to

267 infer the promoter state based on the observed fluorescence intensity curves. The inferred

268 promoter states of the mutant show slightly shorter burst durations compared to its wildtype

269 counterpart (Figure 4C,D, Figure 4 supplement 1C,D). Based on previous studies, burst

270 separation and burst duration can be correlated to bursting parameters, k_{on} and k_{off} (Hoppe et al.

271 2020; Zoller, Little, and Gregor 2018). Using our modeling approach, we extracted the kinetic

272 rates of the promoter returning to an active state from an inactive state (k_{on}) and vice versa (k_{off}).

11
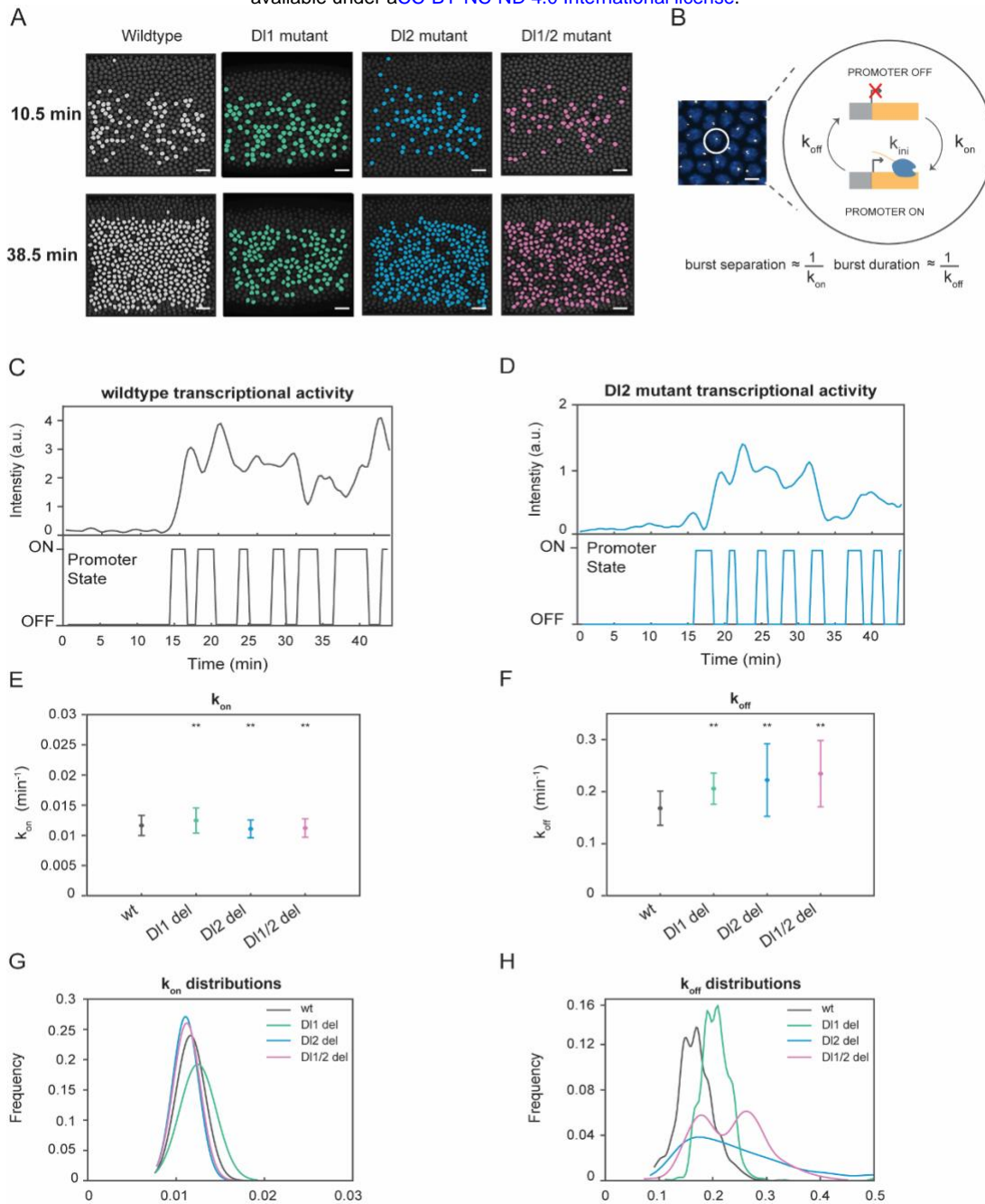
Figure 4. A two-state model reveals differences in k_{off} rates and burst duration

(A) Actively transcribing nuclei are false-colored for early and late NC14. Mutant embryos show more sporadic transcriptional activity in a given frame.

(B) Schematic depicting a single nucleus that can be in an OFF or ON state and switches between the two with rates k_{on} and k_{off}. The rates of k_{on} and k_{off} can be correlated to burst separation and burst duration, respectively.

(C-D) Representative transcriptional trajectory of (C) wildtype and (D) Dl2 mutant with the inferred promoter states derived from the Hidden Markov model (HMM).

(E-F) Plots showing the rates of (E) k_{on} and (F) k_{off}. k_{on} is not significantly affected, whereas k_{off} rates are higher in the mutant embryos. Error bars indicate standard deviation (SD).

(G-H) Probability distributions of (G) k_{on} rates and (H) k_{off} rates for wildtype, Dl1, Dl2, and Dl1/2 mutants. The distribution of k_{on} rates follow a tight normal distribution while the k_{off} distributions vary widely.

Error bars in (E-F) indicate standard deviation (SD).

1124 nuclei from 3 replicate wildtype embryos, 1011 nuclei from 4 replicate Dl1 mutant embryos, 1123 nuclei from four replicate Dl2 mutant embryos, and 943 nuclei from three replicate Dl1/2 mutant embryos were analyzed.

Transcription of the *MS2-yellow* reporter gene is driven by the minimal *sna* distal enhancer.

** denote p<0.001 from the student's t-test.

273   Our results reveal that k_{on} is only slightly affected by the induced mutations, while k_{off} is

274   significantly increased in mutants (Figure 4E,F, Figure 4 supplement 1E,F). Moreover, all of the

275   perturbations do not change the normal distribution trend of k_{on} rates (Figure 4G, Figure 4

276   supplement 1H). However, we observe heterogeneity and high variability in the distribution of k_{off}

277   rates as well as shorter burst durations in the mutated embryos, explaining the bursty and noisy

278   transcriptional activity we observed (Figure 4G,H, Figure 4 supplement 1G,I). This leads us to

279   conclude that the mutations affect the ability of the promoter to remain in the active state, causing

280   it to become more unstable and more likely to revert to the inactive state, supporting the

281   observation of lower mRNA production. In the full distal enhancer, we observe similar stochastic

282   transcriptional activation, where the number of actively transcribing nuclei is about 50% less in

283   the mutants than in the wildtype at any given time (Figure 4 supplement 2A). We also see a similar

284   increase in the rate of k_{off} in the full distal enhancer, with minimal effect on k_{on} (Figure 4 supplement

285   2D-F). The trend in the distributions of the promoter switching rates remains the same as well

286   (Figure 4 supplement 2B-C). Taken together, our data demonstrate that TF-DNA binding

287   modulates mRNA production by increasing the rate of promoter inactivation (koff).

288

289   **Discussion**

290   Organisms have evolved to contain enhancers with multiple binding sites for the same TF, not

291   only for robustness under varying biological conditions, but as a molecular regulatory mechanism.

292   Here, we studied transcriptional dynamics driven by different degrees of TF-DNA interactions

293   through inducing mutations in the *sna* regulatory module. By utilizing quantitative live imaging, we

294   dissected the effects of modulation of TF binding sites and determined that mRNA production of

295   the target gene is severely reduced when a single binding site is mutated. This reduction is mainly

296   due to the decreased transcriptional amplitude (i.e., Pol II loading rate) but is also slightly affected

297   by shorter duration of transcription, delayed transcriptional activation, and lower probability of

298   activation. Although a previous study demonstrated that an extended enhancer with additional

12

299   binding sites could buffer against the effects of mutating a single TF binding site (López-Rivera et

300   al. 2020), we find that the same effect in the minimal enhancer is also observed in the full distal

301   enhancer. It is interesting to note that despite the presence of additional TF binding sites,

302   modulating a single site can catastrophically reduce gene expression levels. We confirm that the

303   minimal enhancer is the core region that is needed to recapitulate normal *sna* levels and that TFs

304   in that region employ distinct mechanisms to regulate transcription in response to genetic

305   perturbations.

306

307   Moreover, we determined that the TF binding sites in the *sna* enhancer work synergistically to

308   drive the proper pattern and levels of the target gene expression. Cooperativity is a necessary

309   mechanism by which a hub of weaker sites can coordinate to synergistically generate the correct

310   expression pattern and levels in a developing embryo. In the context of *sna*, the *sna* enhancer

311   only contains weak Dl binding sites, since high affinity Dl sites would cause *sna* to be expressed

312   in nuclei with intermediate Dl levels, repressing *short gastrulation* (*sog*) expression in the region

313   and preventing those cells from developing into neuroectoderm (Hong et al. 2008). Hence, it is

314   crucial that the *sna* enhancer contains only weak Dl binding sites to drive expression exclusively

315   in the region with high Dl concentration (i.e., mesoderm). Indeed, previous works have shown that

316   other enhancers also utilize weak, sub-optimal binding sites to drive specific target gene

317   expression. It was determined that despite the *shavenbaby* enhancers containing low-affinity

318   binding sites, a microenvironment of high concentrations of Ubx and other cofactors can mediate

319   efficient and specific transcription of the target locus (Tsai et al. 2017). Moreover, a single

320   optimized Dl binding site in the *t48* enhancer resulted in earlier activity and ectopic expression

321   patterns (Keller et al. 2020). Suboptimization of enhancers was shown to be an important

322   characteristic of gene regulation to drive restricted expression, whereas optimizing TF motifs

323   resulted in the loss of specificity and an increase in aberrant transcriptional activity (Farley et al.

13

324   2015). We propose that the *sna* enhancer utilizes synergy among multiple weak binding sites to

325   drive stable and robust expression of *sna* in its narrow expression domain.

326   Interestingly, we found that the TF binding site mutations affect the rate of the promoter switching

327   OFF. The heterogeneity in k_{off} rates confirms that the mutations abolish the ability of the embryo

328   to develop robustly by causing promoter instability and shorter transcription windows, leading to

329   overall lower mRNA production. As a result of higher k_{off} rates, the mutant embryos have fewer

330   actively transcribing nuclei within the domain at any given time point (Figure 4A, Figure 4

331   supplement 1A, Figure 4 supplement 2A, Video 3,4). Furthermore, the shallower gradient of the

332   expression pattern highlights the role of TFs in controlling the sharpness of the expression

333   gradient, potentially affecting the robustness in germ layer formation (Figure 1H,K). In sum, we

334   believe that multiple TF binding sites are imperative not only for pattern formation but also for

335   eliminating extrinsic and intrinsic variabilities that may occur during development.

336

337   We illustrate that the minimal enhancer is an adequate model system to study transcription

338   kinetics. We note that although it may not always be possible to generalize the effects of mutations

339   from a reporter construct to the endogenous setting, we can still gain valuable insights and

340   broaden our understanding of transcription regulation. Since *sna* is responsible for mesoderm

341   formation as well as for the repression of other patterning genes like *sog* that specify

342   neuroectoderm, it will be interesting to characterize the phenotypic effects of these mutations.

343   Specifically, if the mutation causes 65% reduction in *sna* activity endogenously, would the

344   developing embryo undergo proper gastrulation and remain viable? However*,* since *sna* has at

345   least two well-characterized enhancers (proximal and distal) that compensate for each other,

346   investigating the phenotypic effects of endogenously modulating TF binding sites remains

347   challenging. In order to correlate transcriptional dynamics with downstream development it will be

348   critical to carefully design experiments that will disentangle the contributions of the individual

349   enhancers and the role of specific TF binding sites.

350

351 Moreover, the *sna* enhancer contains weaker binding sites for Dl and hence is activated by high

352 concentrations of Dl. For this reason, it will be of interest to note how the induced mutations affect

353 *sna* activity in the presence of reduced maternally deposited Dl levels. While Dl heterozygotes

354 flies are viable and fertile, analyzing development under reduced Dl level conditions may reveal

355 effects on cell-to-cell variability in transcriptional activity. Lastly, the spatial arrangement of the TF

356 binding may also play a role in ensuring normal development. Mutation of the Dl1 site (Figure 1A)

357 seems to cause earlier transcriptional activation, which may indicate a potential competing

358 conformation due to the close proximity between the two Dl sites (Dl1 and Dl2).

359

360 In this work, we demonstrate that TFs can regulate transcriptional dynamics by tuning bursting

361 parameters and modulating transcriptional activity in response to genetic perturbations. Using our

362 quantitative live imaging platform, we find that low-affinity TF binding sites can create an

363 environment of increased transcriptional activity to drive localized, specific, and sharp expression

364 patterns. The evidence of a dual modality of regulation and synergy highlights the importance of

365 moving beyond fixed tissue studies and focusing on experiments that can tease apart subtle

366 kinetic changes that occur during development. Collectively, our findings provide novel insights

367 into enhancer-mediated transcriptional dynamics and expand our understanding of enhancer-TF

368 binding through a combination of experimental and modeling approaches.

369

370 **Materials and methods**

371 **Motif scanning**

372 TF binding sites were found through the FIMO (Find Individual Motif Occurrences) (Bailey et al.

373 2015) tool using motifs from (Keller et al. 2020) and JASPAR (Castro-Mondragon et al. 2022).

374 The cut-off p-value for motif match was set to $p<1e-3$. Mutations of the TF binding sites were

375   confirmed by scanning the mutated sequence through FIMO and ensuring that it was no longer

376   recognizable as a motif. The wildtype and mutated sequences are shown in Table 1.

377

378   **Plasmid and transgenic fly generation**

379   The minimal distal *sna* enhancer was characterized in (Ferraro et al. 2016). TF binding sites were

380   mutated using PCR-mediated site-directed mutagenesis and confirmed via Sanger sequencing

381   (Table 1). The mutated enhancers were cloned into a plasmid containing the core 100 bp *sna*

382   promoter, 10 copies of MS2 stem loops, and the *yellow* reporter gene. Transgenic reporter lines

383   were created using PhiC31-mediated integration and the transgene was inserted to the VK33

384   locus (Venken et al. 2006). Injection was performed by the BestGene, Inc.

385

386   **Live imaging**

387   Wild-type embryos were produced by crossing yw;His2Av-mRFP,nanos>MCP-GFP (Fukaya,

388   Lim, and Levine 2016) virgin females to the desired y,w;MS2 males. The embryos from the cross

389   were laid at 25°C, dechorionated, and staged with Halocarbon oil. All images were taken using a

390   Zeiss LSM800 confocal laser scanning microscope. Images were acquired with a Plan-

391   Apochromat 40x1.3 NA oil objective using a 488 nm and 561 nm laser to visualize MCP:GFP and

392   His2Av-mRFP, respectively, with a time resolution of 21s/frame. Images were created using

393   maximum projection of 14 z-stacks with 0.75 µm steps. The same exposure and laser settings

394   were used for all minimal *sna* replicates and a different set of settings were used for all the full

395   distal *sna* replicates. All images were acquired in 16-bits. Images were taken as the embryo

396   entered the 14th nuclear cycle until the embryo began gastrulation.

397

398   **Quantification and Statistical Analysis**

399   All the image processing methods and analyses were implemented in MATLAB

400   (R2018b, MathWorks). Histograms of all the snapshots and movies shown in all figures were

401   adjusted for visualization purposes only. Analysis of all data was performed using raw images. To

402   determine statistical significance, two sample t-tests were performed. ** indicates $p<0.001$.

403

404   **Image analysis**

405   Segmentation, nuclei tracking, and MS2 signal extraction were performed as described in (Syed

406   et al. 2021). Actively transcribing nuclei were labeled if they exceeded a predetermined

407   fluorescence intensity threshold. mRNA production was calculated by integrating under the

408   fluorescence intensity trajectories of actively transcribing nuclei. Activation time was defined as

409   the time at which the MS2 signal increased beyond the threshold. Transcription duration was

410   calculated to be the time a nucleus was above the given threshold. The mean transcriptional

411   amplitude was determined by the averaging of the MS2 signal for all transcriptionally active nuclei.

412   The average transcriptional trajectory was obtained by averaging the intensity of all active nuclei

413   at each timepoint. The sharpness of the expression gradient was determined by finding the

414   maximum derivative of the mRNA production curves. Spatial analysis was performed by dividing

415   the embryo into 16 bins along the dorsoventral axis. All the nuclei data within each bin was

416   averaged to obtain the plots.

417

418   **Equilibrium binding model**

419   The thermodynamic model utilized in this study is built on those described in (Eck et al. 2020;

420   Kanodia et al. 2012). Concentrations of nuclear DI were assumed to follow a normal distribution.

421   Twi concentration was calculated from (Lim et al. 2015) and normalized. The dissociation

422   constants were chosen to reflect the relative p-values obtained from the FIMO analysis, correlated

423   to the affinity of each binding site. Assuming that the microstates are in equilibrium, the probability

424   of transcription occurring is given by Equation 1:

425    $p_{bound} =$

426

427
$$\frac{\frac{C_A}{K_A} + \frac{C_B}{K_B} + \frac{C_C}{K_C} + \frac{C_D}{K_D} + \omega_1\frac{C_A C_B}{K_A K_B} + \omega_2\frac{C_B C_C}{K_B K_C} + \omega_3\frac{C_A C_C}{K_A K_C} + \omega_4\frac{C_A C_D}{K_A K_D} + \omega_5\frac{C_B C_D}{K_B K_D} + \omega_6\frac{C_C C_D}{K_C K_D} + \omega_7\frac{C_A C_B C_C}{K_A K_B K_C} + \omega_8\frac{C_A C_B C_D}{K_A K_B K_D} + \omega_9\frac{C_B C_C C_D}{K_B K_C K_D} + \omega_{10}\frac{C_A C_C C_D}{K_A K_C K_D} + \omega_{11}\frac{C_A C_B C_C C_D}{K_A K_B K_C K_D}}{1 + \frac{C_A}{K_A} + \frac{C_B}{K_B} + \frac{C_C}{K_C} + \frac{C_D}{K_D} + \omega_1\frac{C_A C_B}{K_A K_B} + \omega_2\frac{C_B C_C}{K_B K_C} + \omega_3\frac{C_A C_C}{K_A K_C} + \omega_4\frac{C_A C_D}{K_A K_D} + \omega_5\frac{C_B C_D}{K_B K_D} + \omega_6\frac{C_C C_D}{K_C K_D} + \omega_7\frac{C_A C_B C_C}{K_A K_B K_C} + \omega_8\frac{C_A C_B C_D}{K_A K_B K_D} + \omega_9\frac{C_B C_C C_D}{K_B K_C K_D} + \omega_{10}\frac{C_A C_C C_D}{K_A K_C K_D} + \omega_{11}\frac{C_A C_B C_C C_D}{K_A K_B K_C K_D}}$$

428

429   where C_i is the concentration of a TF, K_i is the dissociation constant, and ω_i is the cooperativity

430   factor. To find the minimum of the nonlinear multivariable functions in the previous equation, we

431   utilized a nonlinear programming solver, *fmincon*. The solver returns a vector of cooperativity

432   values that minimize the objective function. The objective function uses the root mean square

433   error between the wildtype and mutant conditions to determine the cooperativity terms that would

434   satisfy the constraints (i.e., mutant condition must have 65% reduction in expression level

435   compared to the wildtype). A stable solution was defined once the solution converged and the

436   solver returned cooperativities that satisfied the objective function and constraints within a step

437   tolerance of 1e-10. Using these evaluated cooperativities, curves were generated to predict

438   mRNA production. In the case of no cooperativity (Figure 3B), all cooperativity values were set to

439   1 and the results were plotted.

440

441   **Two-state model**

442   Two-state model fitting is similar to that described in (Keller et al. 2020). Transcriptional

443   trajectories were smoothened using local regression (LOESS) method. Each trajectory from a

444   given nucleus was converted into a binary plot indicating promoter ON (1) and promoter OFF (0)

445   states as described below. The slope between two consecutive time-points of active transcription

446   was obtained to define promoter ON and OFF states. Time points with positive slope were

447   considered as ON promoter states (1), while those with a negative slope were assumed as OFF

448   promoter states (0). This binary data was used as the input for the Baum-Welch based HMM.

449   Initial transition probabilities were assumed to be equal (i.e., 0.5). These probabilities were

450   adjusted in each iteration to individual burst traces until they converged. The Viterbi algorithm was

451   used to determine the most likely sequence of (ON/OFF) promoter states (shown in Figure 4C,D).

452   Burst separation and burst duration were correlated to k_{on} and k_{off}, respectively.

453

Acknowledgements

455   We thank members of the Lim lab for helpful discussions and comments on the manuscript. We

456   especially thank Noel Buitrago for his help in imaging. Dl-venus fly was kindly provided by the

457   Shvartsman Lab at Princeton University. We also thank the FlyBase for providing useful

458   information (Gramates et al. 2022). This study was funded by NIH R35GM133425 awarded to

459   BL.

460

Competing interests

462   The authors declare that there are no competing interests.

463

References

465   Arias, Alfonso Martinez, and Penelope Hayward. 2006. "Filtering Transcriptional Noise during

466   Development: Concepts and Mechanisms." *Nature Reviews Genetics 2006 7:1* 7 (1): 34–44.

467   https://doi.org/10.1038/nrg1750.

468   Bailey, Timothy L., James Johnson, Charles E. Grant, and William S. Noble. 2015. "The MEME

469   Suite." *Nucleic Acids Research* 43 (W1): W39–49. https://doi.org/10.1093/NAR/GKV416.

470   Banerji, Julian, Sandro Rusconi, and Walter Schaffner. 1981. "Expression of a Beta-Globin Gene

471   Is Enhanced by Remote SV40 DNA Sequences." *Cell* 27 (2 Pt 1): 299–308.

472   https://doi.org/10.1016/0092-8674(81)90413-X.

473   Bothma, Jacques P., Hernan G. Garcia, Emilia Esposito, Gavin Schlissel, Thomas Gregor, and

474   Michael Levine. 2014. "Dynamic Regulation of Eve Stripe 2 Expression Reveals

Transcriptional Bursts in Living Drosophila Embryos." *Proceedings of the National Academy of Sciences of the United States of America* 111 (29): 10598–603. https://doi.org/10.1073/PNAS.1410022111/SUPPL_FILE/PNAS.1410022111.SM05.MOV.

Bronson, Jonathan E., Jingyi Fei, Jake M. Hofman, Ruben L. Gonzalez, and Chris H. Wiggins. 2009. "Learning Rates and States from Biophysical Time Series: A Bayesian Approach to Model Selection and Single-Molecule FRET Data." *Biophysical Journal* 97 (12): 3196. https://doi.org/10.1016/J.BPJ.2009.09.031.

Castro-Mondragon, Jaime A., Rafael Riudavets-Puig, Ieva Rauluseviciute, Roza Berhanu Lemma, Laura Turchi, Romain Blanc-Mathieu, Jeremy Lucas, et al. 2022. "JASPAR 2022: The 9th Release of the Open-Access Database of Transcription Factor Binding Profiles." *Nucleic Acids Research* 50 (D1): D165–73. https://doi.org/10.1093/NAR/GKAB1113.

Corrigan, Adam M., Edward Tunnacliffe, Danielle Cannon, and Jonathan R. Chubb. 2016. "A Continuum Model of Transcriptional Bursting." *ELife* 5 (FEBRUARY2016). https://doi.org/10.7554/ELIFE.13051.

Donovan, Benjamin T, Anh Huynh, David A Ball, Heta P Patel, Michael G Poirier, Daniel R Larson, Matthew L Ferguson, and Tineke L Lenstra. 2019. "Live-Cell Imaging Reveals the Interplay between Transcription Factors, Nucleosomes, and Bursting." *The EMBO Journal* 38 (12): e100809. https://doi.org/10.15252/EMBJ.2018100809.

Dufourt, Jeremy, Antonio Trullo, Jennifer Hunter, Carola Fernandez, Jorge Lazaro, Matthieu Dejean, Lucas Morales, et al. 2018. "Temporal Control of Gene Expression by the Pioneer Factor Zelda through Transient Interactions in Hubs." *Nature Communications 2018 9:1* 9 (1): 1–13. https://doi.org/10.1038/s41467-018-07613-z.

Dunipace, Leslie, Anil Ozdemir, and Angelike Stathopoulos. 2011. "Complex Interactions

498   between Cis-Regulatory Modules in Native Conformation Are Critical for Drosophila Snail

499   Expression." *Development* 138 (18): 4075–84. https://doi.org/10.1242/DEV.069146.

500   Eck, Elizabeth, Jonathan Liu, Maryam Kazemzadeh-Atoufi, Sydney Ghoreishi, Shelby Blythe,

501   and Hernan G. Garcia. 2020. "Quantitative Dissection of Transcription in Development

502   Yields Evidence for Transcription Factor-Driven Chromatin Accessibility." *ELife* 9

503   (October): 1–99. https://doi.org/10.7554/ELIFE.56429.

504   Farley, Emma K., Katrina M. Olson, Wei Zhang, Alexander J. Brandt, Daniel S. Rokhsar, and

505   Michael S. Levine. 2015. "Suboptimization of Developmental Enhancers." *Science* 350

506   (6258): 325–28.

507   https://doi.org/10.1126/SCIENCE.AAC6948/SUPPL_FILE/FARLEY.SM.PDF.

508   Ferraro, Teresa, Emilia Esposito, Laure Mancini, Sam Ng, Tanguy Lucas, Mathieu Coppey,

509   Nathalie Dostatni, Aleksandra M. Walczak, Michael Levine, and Mounia Lagha. 2016.

510   "Transcriptional Memory in the Drosophila Embryo." *Current Biology* 26 (2): 212–18.

511   https://doi.org/10.1016/J.CUB.2015.11.058.

512   Fukaya, Takashi, Bomyi Lim, and Michael Levine. 2016. "Enhancer Control of Transcriptional

513   Bursting." *Cell* 166 (2): 358. https://doi.org/10.1016/J.CELL.2016.05.025.

514   Gramates, L Sian, Julie Agapite, Helen Attrill, Brian R Calvi, Madeline A Crosby, Gilberto dos

515   Santos, Joshua L Goodman, et al. 2022. "FlyBase: A Guided Tour of Highlighted Features."

516   *Genetics* 220 (4). https://doi.org/10.1093/GENETICS/IYAC035.

517   Hemavathy, Kirugaval, Xiaodi Hu, Shovon I. Ashraf, Stephen J. Small, and Y. Tony Ip. 2004.

518   "The Repressor Function of Snail Is Required for Drosophila Gastrulation and Is Not

519   Replaceable by Escargot or Worniu." *Developmental Biology* 269 (2): 411–20.

520   https://doi.org/10.1016/j.ydbio.2004.01.029.

521   Hong, Joung Woo, David A. Hendrix, Dmitri Papatsenko, and Michael S. Levine. 2008. "How

522   the Dorsal Gradient Works: Insights from Postgenome Technologies." *Proceedings of the*

523   *National Academy of Sciences of the United States of America* 105 (51): 20072–76.

524   https://doi.org/10.1073/PNAS.0806476105/ASSET/23BB268E-511A-45FD-BD8E-

525   6CC0CCED1BBE/ASSETS/GRAPHIC/ZPQ9990852040003.JPEG.

526   Hoppe, Caroline, Jonathan R. Bowles, Thomas G. Minchington, Catherine Sutcliffe, Priyanka

527   Upadhyai, Magnus Rattray, and Hilary L. Ashe. 2020. "Modulation of the Promoter

528   Activation Rate Dictates the Transcriptional Response to Graded BMP Signaling Levels in

529   the Drosophila Embryo." *Developmental Cell* 54 (6): 727-741.e7.

530   https://doi.org/10.1016/J.DEVCEL.2020.07.007.

531   Houchmandzadeh, Bahram, Eric Wieschaus, and Stanislas Leibler. 2002. "Establishment of

532   Developmental Precision and Proportions in the Early Drosophila Embryo." *Nature 2002*

533   *415:6873* 415 (6873): 798–802. https://doi.org/10.1038/415798a.

534   Ip, Y T, R E Park, D Kosman, K Yazdanbakhsh, and M Levine. 1992. "Dorsal-Twist Interactions

535   Establish Snail Expression in the Presumptive Mesoderm of the Drosophila Embryo."

536   *Genes & Development* 6 (8). https://doi.org/10.1101/gad.6.8.1518.

537   Kanodia, Jitendra S., Hsiao Lan Liang, Yoosik Kim, Bomyi Lim, Mei Zhan, Hang Lu, Christine

538   A. Rushlow, and Stanislav Y. Shvartsman. 2012. "Pattern Formation by Graded and

539   Uniform Signals in the Early Drosophila Embryo." *Biophysical Journal* 102 (3): 427–33.

540   https://doi.org/10.1016/J.BPJ.2011.12.042.

541   Keller, Samuel H., Siddhartha G. Jena, Yuji Yamazaki, and Bomyi Lim. 2020. "Regulation of

542   Spatiotemporal Limits of Developmental Gene Expression via Enhancer Grammar."

543   *Proceedings of the National Academy of Sciences of the United States of America* 117 (26):

544   15096–103.

545   https://doi.org/10.1073/PNAS.1917040117/SUPPL_FILE/PNAS.1917040117.SM04.MOV.

546   Kosman, David, Y. Tony Ip, Michael Levine, and Kavita Arora. 1991. "Establishment of the

547   Mesoderm-Neuroectoderm Boundary in the Drosophila Embryo." *Science* 254 (5028): 118–

548   22. https://doi.org/10.1126/science.1925551.

549   Lammers, Nicholas C., Vahe Galstyan, Armando Reimer, Sean A. Medin, Chris H. Wiggins, and

550   Hernan G. Garcia. 2020. "Multimodal Transcriptional Control of Pattern Formation in

551   Embryonic Development." *Proceedings of the National Academy of Sciences of the United*

552   *States of America* 117 (2): 836–47.

553   https://doi.org/10.1073/PNAS.1912500117/SUPPL_FILE/PNAS.1912500117.SM07.AVI.

554   Leptin, M. 1991. "Twist and Snail as Positive and Negative Regulators during Drosophila

555   Mesoderm Development." *Genes & Development* 5 (9): 1568–76.

556   https://doi.org/10.1101/GAD.5.9.1568.

557   Liang, Hsiao Lan, Chung Yi Nien, Hsiao Yun Liu, Mark M. Metzstein, Nikolai Kirov, and

558   Christine Rushlow. 2008. "The Zinc-Finger Protein Zelda Is a Key Activator of the Early

559   Zygotic Genome in Drosophila." *Nature* 456 (7220): 400–403.

560   https://doi.org/10.1038/NATURE07388.

561   Lim, Bomyi, Carmeline J Dsilva, Thomas J Levario, Hang Lu, Trudi Schüpbach, Ioannis G

562   Kevrekidis, and Stanislav Y Shvartsman. 2015. "Dynamics of Inductive ERK Signaling in

563   the Drosophila Embryo." https://doi.org/10.1016/j.cub.2015.05.039.

564   Long, Hannah K., Sara L. Prescott, and Joanna Wysocka. 2016. "Ever-Changing Landscapes:

565   Transcriptional Enhancers in Development and Evolution." *Cell* 167 (5): 1170–87.

566   https://doi.org/10.1016/J.CELL.2016.09.018.

567 López-Rivera, Francheska, Olivia K. Foster Rhoades, Ben J. Vincent, Edward C.G. Pym,

568   Meghan D.J. Bragdon, Javier Estrada, Angela H. DePace, and Zeba Wunderlich. 2020. "A

569   Mutation in the Drosophila Melanogaster Eve Stripe 2 Minimal Enhancer Is Buffered by

570   Flanking Sequences." *G3: Genes|Genomes|Genetics* 10 (12): 4473.

571   https://doi.org/10.1534/G3.120.401777.

572 Mir, Mustafa, Armando Reimer, Jenna E. Haines, Xiao Yong Li, Michael Stadler, Hernan

573   Garcia, Michael B. Eisen, and Xavier Darzacq. 2017. "Dense Bicoid Hubs Accentuate

574   Binding along the Morphogen Gradient." *Genes & Development* 31 (17): 1784–94.

575   https://doi.org/10.1101/GAD.305078.117.

576 Monod, Jacque, Jeffries Wyman, and Jean Pierre Changeux. 1965. "On the Nature of Allosteric

577   Transitions: A Plausible Model." *Journal of Molecular Biology* 12 (1): 88–118.

578   https://doi.org/10.1016/S0022-2836(65)80285-6.

579 Park, Jeehae, Javier Estrada, Gemma Johnson, Ben J Vincent, Chiara Ricci-Tam, Meghan DJ

580   Bragdon, Yekaterina Shulgina, et al. 2019. "Dissecting the Sharp Response of a Canonical

581   Developmental Enhancer Reveals Multiple Sources of Cooperativity." *ELife* 8 (June).

582   https://doi.org/10.7554/ELIFE.41266.

583 Perry, Michael W., Alistair N. Boettiger, Jacques P. Bothma, and Michael Levine. 2010.

584   "Shadow Enhancers Foster Robustness of Drosophila Gastrulation." *Current Biology : CB*

585   20 (17): 1562. https://doi.org/10.1016/J.CUB.2010.07.043.

586 Ramos, Andrea I., and Scott Barolo. 2013a. "Low-Affinity Transcription Factor Binding Sites

587   Shape Morphogen Responses and Enhancer Evolution." *Philosophical Transactions of the*

588   *Royal Society B: Biological Sciences* 368 (1632). https://doi.org/10.1098/RSTB.2013.0018.

589 ———. 2013b. "Low-Affinity Transcription Factor Binding Sites Shape Morphogen Responses

590   and Enhancer Evolution." *Philosophical Transactions of the Royal Society B: Biological*

591   *Sciences* 368 (1632). https://doi.org/10.1098/rstb.2013.0018.

592   Reiter, Franziska, Sebastian Wienerroither, and Alexander Stark. 2017. "Combinatorial Function

593   of Transcription Factors and Cofactors." *Current Opinion in Genetics & Development* 43

594   (April): 73–81. https://doi.org/10.1016/J.GDE.2016.12.007.

595   Rembold, Martina, Lucia Ciglar, J. Omar Yáñez-Cuna, Robert P. Zinzen, Charles Girardot,

596   Ankit Jain, Michael A. Welte, Alexander Stark, Maria Leptin, and Eileen E.M. Furlong.

597   2014. "A Conserved Role for Snail as a Potentiator of Active Transcription." *Genes &*

598   *Development* 28 (2): 167. https://doi.org/10.1101/GAD.230953.113.

599   Rodriguez, Joseph, and Daniel R. Larson. 2020. "Transcription in Living Cells: Molecular

600   Mechanisms of Bursting." *Https://Doi.Org/10.1146/Annurev-Biochem-011520-105250* 89

601   (June): 189–212. https://doi.org/10.1146/ANNUREV-BIOCHEM-011520-105250.

602   Senecal, Adrien, Brian Munsky, Florence Proux, Nathalie Ly, Floriane E. Braye, Christophe

603   Zimmer, Florian Mueller, and Xavier Darzacq. 2014. "Transcription Factors Modulate C-

604   Fos Transcriptional Bursts." *Cell Reports* 8 (1): 75–83.

605   https://doi.org/10.1016/J.CELREP.2014.05.053.

606   Spitz, François, and Eileen E.M. Furlong. 2012. "Transcription Factors: From Enhancer Binding

607   to Developmental Control." *Nature Reviews Genetics 2012 13:9* 13 (9): 613–26.

608   https://doi.org/10.1038/nrg3207.

609   Syed, Sahla, Henry Wilky, João Raimundo, Bomyi Lim, and Amanda A. Amodeo. 2021. "The

610   Nuclear to Cytoplasmic Ratio Directly Regulates Zygotic Transcription in *Drosophila*

611   through Multiple Modalities." *Proceedings of the National Academy of Sciences* 118 (14).

612   https://doi.org/10.1073/pnas.2010210118.

613   Tsai, Albert, Anand K. Muthusamy, Mariana R.P. Alves, Luke D. Lavis, Robert H. Singer,

614   David L. Stern, and Justin Crocker. 2017. "Nuclear Microenvironments Modulate

615   Transcription from Low-Affinity Enhancers." *ELife* 6 (November).

616   https://doi.org/10.7554/ELIFE.28975.

617   Venken, Koen J.T., Yuchun He, Roger A. Hoskins, and Hugo J. Bellen. 2006. "P[Acman]: A

618   BAC Transgenic Platform for Targeted Insertion of Large DNA Fragments in D.

619   Melanogaster." *Science (New York, N.Y.)* 314 (5806): 1747–51.

620   https://doi.org/10.1126/SCIENCE.1134426.

621   Zeitlinger, Julia, Robert P. Zinzen, Alexander Stark, Manolis Kellis, Hailan Zhang, Richard A.

622   Young, and Michael Levine. 2007. "Whole-Genome ChIP-Chip Analysis of Dorsal, Twist,

623   and Snail Suggests Integration of Diverse Patterning Processes in the Drosophila Embryo."

624   *Genes & Development* 21 (4): 385–90. https://doi.org/10.1101/GAD.1509607.

625   Zoller, Benjamin, Shawn C. Little, and Thomas Gregor. 2018. "Diverse Spatial Expression

626   Patterns Emerge from Unified Kinetics of Transcriptional Bursting." *Cell* 175 (3): 835-

627   847.e25. https://doi.org/10.1016/J.CELL.2018.09.056.

628